RESEARCH ARTICLE

# Tensile behavior of 6063/Al$_2$o$_3$ particulate metal matrix composites fabricated by investment casting process

Chennakesava Reddy. A, Essa Zitoun
Professor, Department of Mechanical Engineering, JNTUH College of Engineering
Hyderabad – 500085, Andhra Pradesh, India
dr_acreddy@yahoo.com

## ABSTRACT

The use of investment casting process has been studied to fabricate 6063/Al$_2$O$_3$ metal matrix composites. The tensile properties have been evaluated. The EDS report confirms the presence of Al$_5$Cu$_2$Mg$_8$Si$_6$, Al$_4$CuMg$_5$Si$_4$ and Mg$_2$Si compounds in the 6063/Al$_2$O$_3$ composites. The yield strength and fracture strength increase with increase in volume fraction of Al$_2$O$_3$, whereas ductility decreases. The fracture mode is ductile in 10% volume fraction composite and the brittle fracture is observed in 20% and 30% volume fraction composites.

**Key words**: investment casting process, colloidal silica, 6063, alumina, tensile

## 1. Introduction

Particulate reinforced metal matrix composite (PRMMC) consists of a uniform distribution of strengthening ceramic particles embedded within a metal matrix. Divecha et al., 1981 have expressed that the PRMMC exhibits higher strength and stiffness, in addition to isotropic behavior at a lower density, when compared to the un-reinforced matrix material. Chawla, 1997 have found aluminum alloy based metal matrix composites an attractive and viable nominee for automobile and aerospace applications.

The mechanical properties of aluminium alloys reinforced with ceramic particulates are known to be influenced by the particle size and the volume fraction. Arsenault, 1984 has concluded from the series of experiments that 0.2% proof stress and ultimate tensile strength tend to increase, and toughness and ductility decrease with increasing volume fraction of particulate or decreasing particle size. Zhou and Xu, 1997 have used the stir casting method as an alternative low cost liquid processing technique to produce PRMMC. Stir casting route also ensures that undamaged reinforcement materials are attained. Hashim et al., 1999 have made this type of processing in commercial use for particulate Al-based composites. A two-step stirring was developed for homogeneous particle distribution to fabricate particulate metal matrix composites.

The objective of the present work was to study the influence of microstructure (as-cast and heat treatment conditions), volume fraction of alumina reinforcement on the tensile properties, and fracture behavior of 6063 aluminium alloy metal matrix composite reinforced with alumina (Al$_2$O$_3$). In the present work, the investment casting process was implemented to fabricate alumina particulate reinforced metal matrix composites.

## 2. Experimental Procedure

The chemical composition of 6063 matrix alloy is given in Table 1. The properties of the matrix alloy are given in Table 2. The volume fractions of $Al_2O_3$ particulate reinforcement are 10%, 20% and 30%. The particle size of $Al_2O_3$ is 10 μm.

**Table 1:** Chemical composition of matrix alloy 6063

| Alloy | Composition determined spectrographically, % | | | | | | | | |
|-------|------|-------|-------|--------|--------|------|--------|-------|--------|
|       | Al   | Si    | Fe    | Cu     | Ti     | Mg   | Mn     | Zn    | Cr     |
| 6063  | 98.2 | 0.271 | 0.325 | 0.0047 | 0.0376 | 0.58 | 0.0076 | 0.076 | 0.0005 |

**Table 2**: Mechanical properties of matrix alloy 6063

| Matrix Material | Density, g/cc | Modulus of Elasticity, GPa | Ultimate Tensile strength, MPa | Elongation, % |
|-----------------|---------------|----------------------------|--------------------------------|---------------|
| 6063            | 2.70          | 68.9                       | 172                            | 22            |
| 6063(T6)        | 2.70          | 68.1                       | 245                            | 12            |
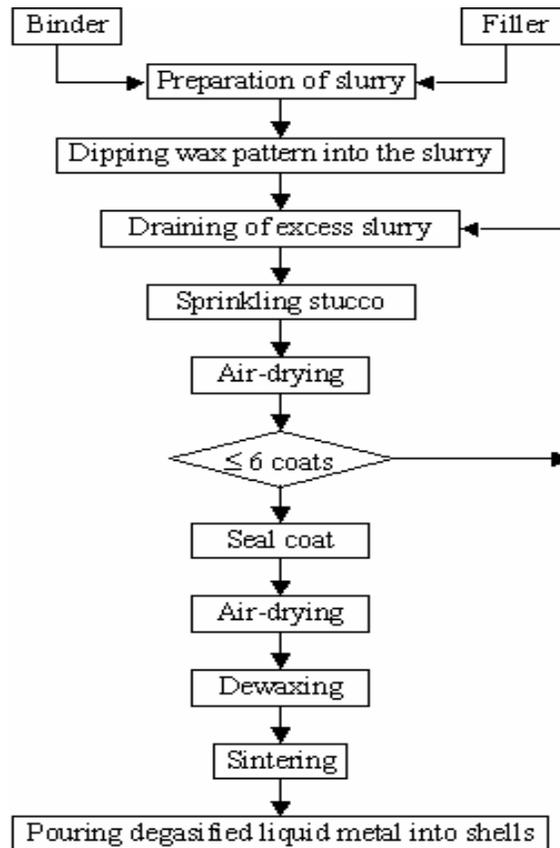


**Figure 1:** Flowchart of investment casting process

## 2.1 Preparation of ceramic shells, melt and metal matrix composites

Reddy et al., 1996 have developed the ceramic shell process using colloidal silica as a binder for casting composite materials. Dip-coating slurries were prepared by adding the refractory filler to the liquid binder using sufficient agitation to breakup agglomerates and thoroughly wet and disperse the filler. Colloidal silica binder and alumina filler (particles of size 45 μm) were used to prepare dip-coating slurring. The colloidal concentration in the binder was 30%. The filler to binder ratio was 0.65. Ceramic shells were made by applying a series of ceramic coating to the patterns. The wax pattern was first dipped into the dip-coating slurry bath. The pattern was then withdrawn from the slurry and manipulated to drain-off excess slurry and to produce uniform layer. The wet layer was immediately stuccoed with coarse silica sand. Each coating was allowed to dry for four hours in the open air. The operations of coating, stuccoing, and drying were repeated six times. The seventh coat was left unstuccoed to avoid the occurrence of loose particles on the shell surface. The first two coats were stuccoed with a sand of AFS fineness number 120 and the next four coats were stuccoed with coarse sand of AFS fineness number 50. After all coats the shells were air dried for 24 hours (figure 1).

Al alloys were melted in a resistance furnace. The crucibles were made of graphite. The melting losses of alloy constituents were taken into account while preparing the charge. The charge was fluxed with coverall to prevent dressing. The molten alloy was degasified by tetrachlorethane (in solid form). The crucible was taken out of the furnace and modified with sodium. Then the liquid melt was allowed to cool down just below the liquidus temperature to bring the melt semi solid state. At this stage, the preheated ($1000^0$C for 1 hour) alumina ($Al_2O_3$) particles were added to the liquid melt. The molten 6061 alloy and $Al_2O_3$ particles are thoroughly stirred manually. After sufficient manual stirring, the semi-solid liquid melt was reheated to a fully liquid state in the resistance furnace followed by automatic mechanical stirring using a mixer to make the melt homogenous for about 15 minutes at 200 rpm. The temperature of the melt was measured using a dip type thermocouple. The preheated ($200^0$C) ceramic shell was gravity poured with the liquid melt. The wax pattern, ceramic shell and casting are shown in figure 2.
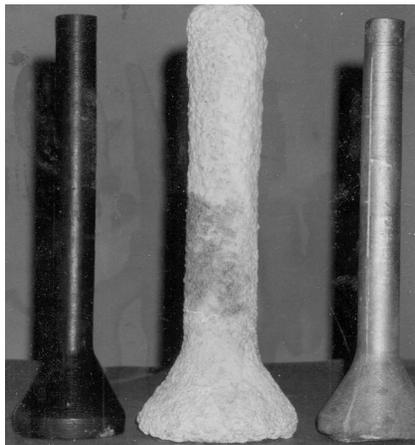


**Figure 2:** Wax pattern, ceramic shell, and casting

RESEARCH ARTICLE                                                    ISSN - 0976-4259

## 2.2 Heat Treatment

Prior to the machining of composite samples, a solution treatment was applied at $550^0$ C for 15 min quenched in cold water, and aged at $150^0$C for 100 hours.

## 2.3 Tensile Tests

The as-cast and heat treated samples were machined to get specimens for tensile test. The shape and dimensions of the tensile specimen are shown in figure 3. The universal testing machine (UTK-E: PC based) was used for the tensile test. The specimens were loaded hydraulically. The loads at which the specimen has reached the yield point and broken were noted down. The extensometer was used to measure the elongation.
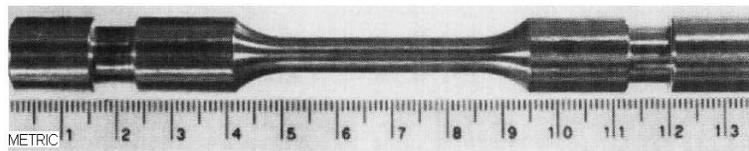


Figure 3: Standard 6 mm diameter cylindrical tensile specimen

## 2.3 Optical and Scanning Electron Microscopic Analysis

The microscopic structures of the composite samples were revealed by the optical microscopy. The polished specimens were ringed with distilled water and etched with 0.5% HF solution. Fracture surfaces of the deformed/fractured (under tensile loading) test samples were examined in a scanning electron microscope (SEM) to determine the macroscopic fracture mode and to establish the microscopic mechanisms governing fracture. Samples for SEM observation were obtained from the tested specimens by sectioning parallel to the fracture surface and the scanning was carried in IICT (Indian Institute of Chemical Technology - Hyderabad) S-3000N Toshiba. EDS analysis was carried out to find the formation of interfacial compounds in the composites.

## 3. Results and Discussion

Three tensile specimens were tested for each trial. The average values of yield strength, fracture strength (ultimate tensile strength), and ductility in terms of tensile elongation are presented in the graphical forms.

## 3.1 Undeformed microstructure

The optical micrographs illustrating the microstructures of the as-cast and heat-treated $6063/Al_2O_3$ metal matrix composites are shown in figure 4. In the as-cast condition, Al is present both in solid solution with the matrix and precipitated as $Al_{12}Mg_{17}$ phase that is present at and along the grain boundaries. A non-uniform distribution of $Al_2O_3$ particulates through the 6063 metal-matrix with evidence of clustering, or agglomeration is observed. In the as-cast $6063/Al_2O_3$ composite, the phases $Mg_2Si$, MgO and $MgAl_2O_4$ are also seen along the grain boundaries (figure 4a).
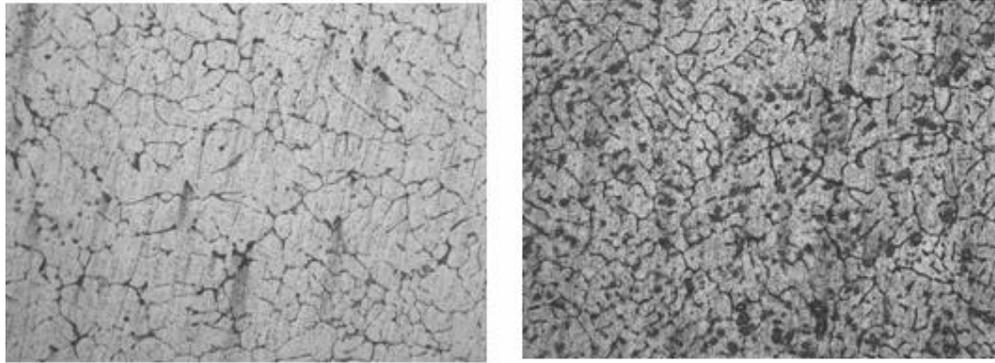
**Figure 4:** Microstructure of as-cast 6063/ $Al_2O_3$ metal matrix composite (volume fraction = 20%) (a) as-cast; (b) heat-treated
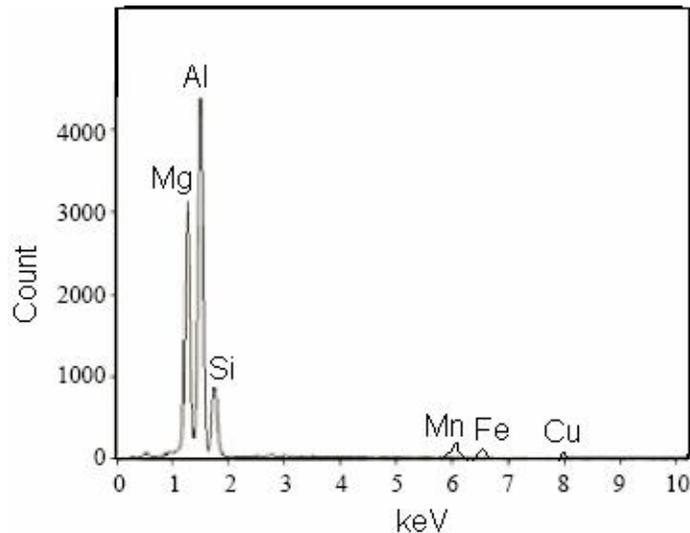


**Figure 5:** EDS analysis of heat treated 6063/$Al_2O_3$ metal matrix composite (volume fraction = 20%)

Magnesium and silicon combine to form a compound magnesium silicide ($Mg_2Si$), which in turn forms a simple eutectic system with aluminum. The microstructure of heat-treated 6063/$Al_2O_3$ composite reveal particles of intermetallics such as $Al_5Cu_2Mg_8Si_6$ and $Al_4CuMg_5Si_4$ precipitated during the heat-treatment (figure 4b). These are brittle in nature. The as-cast microstructure (figure 4a) reveals coarse grain structure whereas the heat-treated microstructure (figure 4b) represents the fine grain structure. The presence of manganese, iron, copper, leads to the formation of (Fe, Mn, Cu)$_3$SiAl$_{12}$ and the presence of magnesium escorts to the formation of $Mg_2Si$ (figure 5).

RESEARCH ARTICLE
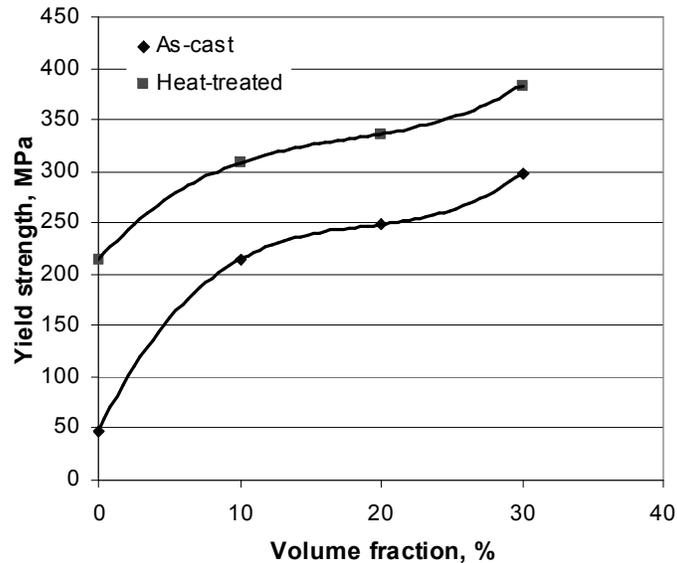


**Figure 6:** Variation of the yield strength with the volume fraction of $Al_2O_3$ particles

## 3.2 Tensile properties

Figure 6 illustrates the influence of volume fraction of $Al_2O_3$ (reinforcement) on the on the yield strength of $6063/Al_2O_3$ Metal matrix composites. The yield strength is defined as the stress corresponding to a plastic strain of 0.2%. The graphs indicate that the yield strength increases with increase in volume fraction of $Al_2O_3$ in the composite. With increasing volume fraction, more load is transferred to the reinforcement which also results in a higher yield strength. This behavior is in agreement with the work carried by Yung et al, 2004. There is an increase of 84% yield strength in the reinforced composite over the as-cast 6063 alloy and an increase of 44% yield strength in the heat treated composite over the heat treated 6063 alloy when the metal matrix alloy 6063 is reinforced with 30% volume fraction of $Al_2O_3$. The yield strength increases after solution treatment. Upon cooling, dislocations form at the matrix/reinforcement interface owing to the thermal mismatch. The tangled dislocations around the agglomeration of the alumina particles could contribute a reinforcement effect in the Al-alloy matrix. According to previous literature (Besterci et al., 1992), the yield strength of the Al-alloy is related the particulate – dislocation interaction by means of the Orowan bowing mechanism. The area between the upper line and the lower line in figure 6 represents the strengthening effect due to dislocations and precipitation hardening. If the agglomeration appears to be bonded to the matrix, the agglomeration can contribute to the strengthening of the composite. The degree of agglomeration increases with the increase in volume fraction.

Figure 7 shows the effect of volume fraction on the fracture strength (ultimate tensile strength). The fracture strength follows the same trend as the yield strength of $6063/Al_2O_3$ composite. There is an increase of 75% fracture strength in the reinforced composite over the as-cast 6063 alloy and an increase of 42% fracture strength in the heat treated composite over the heat treated 6063 alloy when the metal matrix alloy 6063 is reinforced with 30% volume fraction of $Al_2O_3$. The fracture strength is only marginally higher than the yield strength. The increase in fracture strength over the yield strength is 14% of the as-cast $6063/Al_2O_3$

composite having volume fraction of 30%, whereas the increase in fracture strength is 7% of heat-treated $6063/Al_2O_3$ composite having volume fraction of 30%. This indicates that the work hardening rate past yielding is low in the heat-treated composites. An earlier work reported by Chawla and Shen, 2001 that the work hardening rate was a simple function of lower matrix volume (the matrix volume decreases with increase in volume fraction of reinforcement.
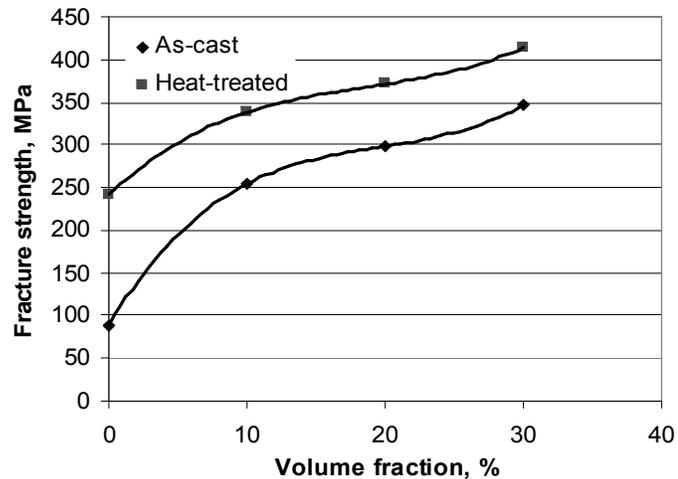


**Figure 7:** Variation of the fracture strength with the volume fraction of $Al_2O_3$ particles

The influence of volume fraction of $Al_2O_3$ on the ductility (measured in terms of tensile elongation) is shown in figure 8. The decrease in the ductility is 76% of the as-cast $6063/Al_2O_3$ composite having volume fraction of 30%, whereas the decrease in the ductility is 74% of heat-treated $6063/Al_2O_3$ composite. The decrease in the ductility can be attributed to the beginning of void nucleation in advance with increasing amount of $Al_2O_3$ reinforcement. It was verified from the work carried out by Arsenault et al, 1991 that the microplasticity took place in the metal matrix composites due to stress concentrations in the matrix at the poles of the reinforcement and/or at sharp corners of the reinforcing particles.
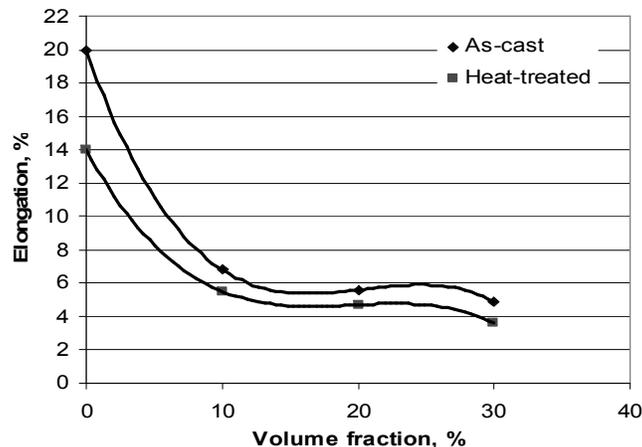


**Figure 8:** Variation of the ductility with the volume fraction of $Al_2O_3$ particles

**RESEARCH ARTICLE**                                                      **ISSN - 0976-4259**
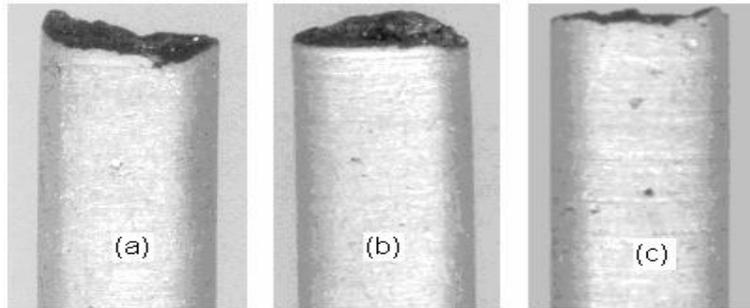


**Figure 9:** Tensile fracture surfaces of 6063/Al$_2$O$_3$ composites (a) 10% Al$_2$O$_3$, (b) 20% Al$_2$O$_3$, and (c) 30% Al$_2$O$_3$

## 4. Fracture Behavior

Figure 9a shows ductile fracture for the 6063/Al$_2$O$_3$ composite (having 10% volume fraction) with no extensive diameter contraction. The existence of the reinforcing Al$_2$O$_3$ particles caused considerable change in the behavior of the fracture process. In figure 10 the dimples are neither uniform nor circular in shape. The matrix-particle decohesion is also observed. The fracture mechanism is ductile, involving the nucleation, growth, and coalescence of voids in the matrix around the Al$_2$O$_3$ particles.

Figure 9b reveals brittle fracture for the 6063/Al$_2$O$_3$ composite (having 20% volume fraction) with extensive microvoids in the matrix. In figure 11 the dimples are different from those in figure 10 both in size and shape. Figure 11 shows greater percentage matrix-particle decohesion is observed for the 6063/Al$_2$O$_3$ composite (having 20% volume fraction) than that previously observed for the 6063/Al$_2$O$_3$ composite (having 10% volume fraction). The voids grow under both the applied load and the influence of local plastic constraint until a coalescence mechanism is activated, and this followed by the total failure of the specimen.
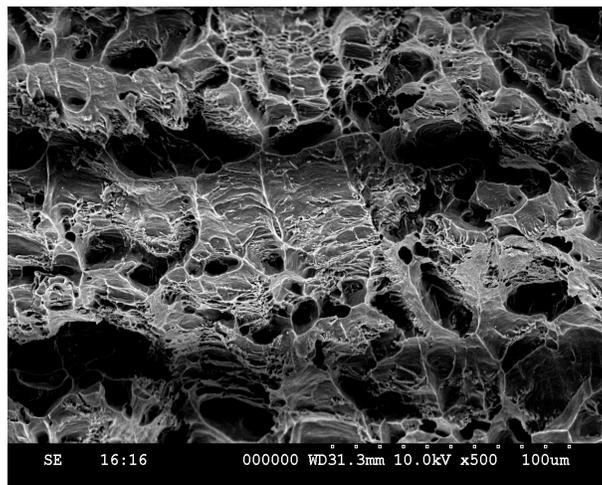


**Figure 10:** SEM fracture surface of heat-treated tensile sample (volume fraction = 10%)

**RESEARCH ARTICLE**                                                                                   **ISSN - 0976-4259**

Figure 9c shows the fracture surface of 6063/Al$_2$O$_3$ composite (having 30% volume fraction) composite. The fracture surface appears to be flat and normal to axis of loading. On a microscopic scale (figure 12), the fracture surface appears to contain many microvoids in the matrix. The matrix-particle decohesion is also observed for this composite (figure 12), but more extensively than those observed for the 10%, 20% volume fraction composites. The void coalescence occurs when the void elongates to the initial intervoid spacing. This leads to the dimpled appearance of the fractured surfaces. Brittle fracture of this composite indicates that void growth and coalescence occurred rapidly. The fracture process in high volume fraction (more than 20%) 6063/ Al$_2$O$_3$ composites is very much localized and the failure path in these composites is through the matrix-particle interface rupturing to the reinforcement particle cracking. The presence of Al$_2$O$_3$ reinforcement particles reduces the average distance in the composite by providing strong barriers to dislocation motion (figure 12).
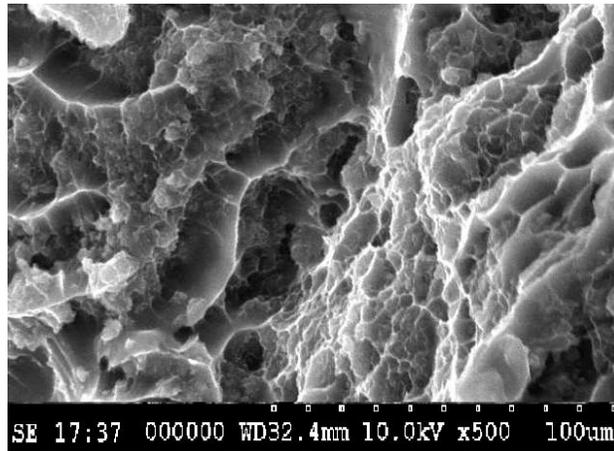


**Figure 11:** SEM fracture surface of heat-treated tensile sample (volume fraction = 20%)
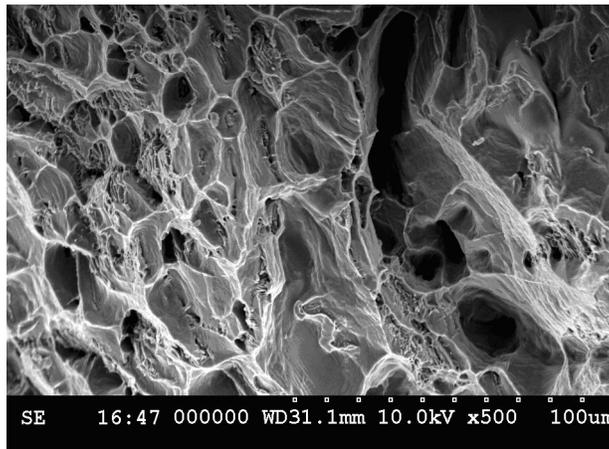


**Figure 12:** SEM fracture surface of heat-treated tensile sample (volume fraction = 30%)

RESEARCH ARTICLE                                                                    ISSN - 0976-4259

## 5. Conclusions

The micrographs of as-cast and heat treated 6063/ $Al_2O_3$ composites indicate random distribution of $Al_2O_3$ particles in the metal matrix composites. The EDS report confirms the presence of $Al_5Cu_2Mg_8Si_6$, $Al_4CuMg_5Si_4$ and $Mg_2Si$ compounds in the 6063/$Al_2O_3$ composites. The yield strength and fracture strength increase with increase in volume fraction of $Al_2O_3$, whereas ductility of 6063/ $Al_2O_3$ composites decreases. The fracture mode is ductile in 10% volume fraction composite and the brittle fracture is observed in 20% and 30% volume fraction composites.

## Acknowledgements

## References

1. Arsenault R.J., 1984, The Strengthening of Aluminum Alloy 6061 by Fiber and Platelet Silicon Carbide, Material Science and Engineering, 64 (2), pp.171–81.

2. Arsenault R.J., Wang L., and Feng C.R., 1991, Strengthening of Composites due to Microstructural Changes in the Matrix, Acta Metallurgica, 39, pp.47-57.

3. Besterci M., Slesar M., and Jangg G., 1992, Structure and Properties of Dispersion Hardened Al-$Al_4C_3$ Materials, Powder Metallurgy International, 24, pp.27-32.

4. Chawla N., and Shen Y.L., 2001, Mechanical Behavior of Particle Reinforced Metal Matrix Composites, Advanced Engineering Materials, 3, pp.357-370.

5. Divecha A.P., Fishman S.G., and Karmarkar S.D., 1981, Silicon Carbide Reinforced Aluminum – a Formable Composite, Journal of Metals, 33(9), pp.12–17.

6. Hashim J., Looney L., and Hashmi M.S.J., 1999, Metal Matrix Composites: Production by the Stir Casting Method, Journal of Material Processing and Technology, 92, pp. 1-7.

7. K.K. Chawla., 1997, Composite Materials: Science and Engineering. 2nd edition, Springer-Verlag, New York, 102-104.

8. Reddy A.C., Niranjan H.B., and Murti A.R.V., 1996, Optimization of Investment Shell Mould using Colloidal Silica Binder, Journal of Engineering and Materials Sciences, 3, pp.180-184.

9. Yung C.K., and Chan S.L.I., 2004, Tensile Properties of Nanometric $Al_2O_3$ Particulate Reinforced Aluminium Matrix Composites, Journal of Materials Chemistry and Physics, 85, pp.438-443.

10. Zhou W., and Xu Z.M., 1997, Casting of SiC Reinforced Metal Matrix Composites, Journal of Material Processing and Technology, 63, pp.358-363.